Propagation of waves through a line of discontinuity in two-dimensional excitable media: Refraction and reflection of autowaves

Pavel K. Brazhnik and John J. Tyson
Department of Biology, Virginia Polytechnic Institute and State University, Blacksburg, Virginia 24061
(Received 24 January 1996)

A theoretical study of excitation waves propagating in two-dimensional excitable media through the boundary line between two areas with different properties is presented and compared with available experimental evidences. Based on the kinematic approach, a complete set of steady wave-front configurations have been constructed for unbounded media, for media confined in a half-plane, and for a strip. Our results confirm the experimentally observed Snell's law for incident and refracted autowaves, and the existence of a critical angle for total internal reflection. [S1063-651X(96)02108-3]

PACS number(s): 03.40.Kf

I. INTRODUCTION

The dynamics of wave fronts propagating in two-dimensional (2D) and three-dimensional (3D) excitable media (EM) have become a focus of much study since the observation of nontrivial spirallike patterns in chemical reactions [e.g., Belousov-Zhabotinsky (BZ) reaction] and neuromuscular tissues [1,2]. Excitation waves (autowaves) in 2D and 3D EM come in a variety of shapes and move in complicated patterns, which still challenge satisfactory theoretical explanations.

Continuous mathematical models of EM are usually formulated in terms of nonlinear parabolic partial differential equations (PDE) [3,4]:

$$\frac{\partial u_i}{\partial t} = D_i \Delta u_i + f_i(u_1, u_2, \ldots, u_m), \tag{1}$$

where $\{u_i\}$ is a set of local kinetic variables determining the state of the EM, D_i are transport coefficients, Δ is the Laplacian operator with respect to space variables, f_i are nonlinear functions of $u_1, u_2, \ldots, u_m$ describing the local kinetics of the system, and the dimension of physical space can be 1, 2, or 3. Usually, system (1) is subject to no-flux (Neumann) boundary conditions

$$\mathrm{grad} u_i|_{\mathrm{boundary}} \cdot \mathbf{n} = 0, \tag{2}$$

where $\mathbf{n}$ is a unit vector normal to the boundary.

The basic features of autowave propagating in EM can be reproduced by two-component models ($m=2$): an excitation variable (u) and a recovery variable (v). It is arranged that a single equilibrium state (u^e, v^e) exists. Small perturbations from the equilibrium state return directly to (u^e, v^e), but suprathreshold perturbations in the system invoke an excitation cycle which results in the generation of a propagating pulse (solitary autowave) whose leading front corresponds to the transition wave from the state of rest to an excited state, and whose trailing front corresponds to a return of the system to the equilibrium state. The recovery variable (v) is responsible for the appearance of the trailing front and the temporarily unexcitable region just behind an excitation front. Important particular cases of such systems are the Oregonator and the FitzHugh-Nagumo (FHN) equations used to describe (respectively) the autocatalytic BZ reaction, and excitation waves in nerve and muscle tissue [5].

In homogeneous EM, an isolated planar autowave propagates with constant amplitude, shape, and speed. A periodic train of planar autowaves propagates with amplitude, shape, and speed that depend on the spacing between the waves (dispersion) [6,7]. If a wave front is curved, its speed depends on its curvature [6,8,9]. Because a wave front of excitation is always followed by a zone of inexcitability, colliding autowaves tend to annihilate each other and disappear at boundaries, which distinguishes them significantly from electromagnetic or soliton waves [10,11].

Recently considerable attention has been attracted to the study of autowaves propagating in inhomogeneous media [4,12–17]. Natural EM are often inhomogeneous, due to temperature or concentration gradients, and controlled inhomogeneities can be created with ultraviolet or visible light [12,13,17,18], ultrasonic radiation [19], or electrical fields [14]. For inhomogeneous media the local kinetics vary in space, that is, the functions $f_{1,2}$ depend, apart from the state variables $\{u,v\}$, also on the space variables $\{x,y,z\}$. If the transport coefficients are space dependent as well $D_i = D_i(x,y,z)$ then the first term on the right-hand side of (1) must be replaced by $\mathrm{div}(D_i \mathrm{grad} u_i)$.

The reaction of a wave front to an inhomogeneity depends on the size of the perturbed area of EM. Local defects (like concentration fluctuations, nonexcitable or poorly excitable areas) are inhomogeneities whose sizes are smaller or comparable to the width of an excitation pulse. A wave front may overcome them and recover its shape, but they may also be responsible for breaking fronts and initiating spiral waves (a commonly believed origin of tachycardia [2,20]) [21]. If the density of local defects is large enough, the wave-front pattern can become chaotic [22].

For global inhomogeneity, properties of the medium vary continuously at scales much larger than the width of the excitation pulse, or the medium is divided in large pieces with different properties by negligibly thin boundaries penetrable by excitation waves. In some circumstances, steady-state or nearly steady-state regimes may be expected in such media. For instance, spiral waves drift in globally inhomogeneous media [23], as they do along impenetrable bound-

aries [24]; bell-like waves propagate in a medium with a stripe [13,25,26]; and saw-tooth patterns of crossing waves develop in coupled excitable layers [27].

One of the simplest examples of global inhomogeneity is stratification. In this case, properties of the medium vary in space in one direction only. For instance, a layer of BZ reagent in a petri dish has an oxygen concentration gradient (and a concomitant excitability gradient) from the air-liquid interface to the liquid-glass interface. Waves can also propagate in adjacent excitable layers with different properties. In some cases the property varies abruptly from layer to layer, and the medium can be considered as piecewise constant stratified. In contrast to an impenetrable (no-flux) boundary, the boundary between adjacent excitable layers may be semipenetrable, provided that the excitation does not disappear from layer to layer. The phenomena of autowave propagation in layered EM can be important in biological tissues, marine and lake ecological systems, and multilayer solid state devices (consider, for instance, the practical importance of electromagnetic waves propagating in optical layers). Recent experiments with the BZ reaction [12,13,16,17] and theoretical studies [25,26] have shown that excitation fronts undergo nontrivial transformations in media with piecewise inhomogeneity. Many questions about autowaves propagation in piecewise media remain open. For instance, it has been believed for a long time that autowaves do not reflect from boundaries [28], but recently wave reflection in the BZ reaction has been observed [12,16,29]. Recent theoretical works have shown the possibility of autowave reflection in special circumstances [30,31].

As with other theories of piecewise continuous media, autowave front configurations in piecewise EM are to be constructed from solutions for homogeneous media with appropriate concatenation of the solutions (and their derivatives) along boundary lines. For example, for the EM consisting of two half-planes with different properties abutting along the X axis, the semipenetrable boundary conditions are

$$u_i|_{y=0^+} = u_i|_{y=0^-}, \tag{3}$$

$$D_i\left(\frac{\partial u_i}{\partial y}\right)_{y=0^+} = D_i\left(\frac{\partial u_i}{\partial y}\right)_{y=0^-}. \tag{4}$$

This simple algorithm turns out to be difficult to follow because analytical solutions of the reaction-diffusion system for 2D are not available.

The only theoretical attempt to study autowave refraction and reflection in 2D EM using this recipe was undertaken by Mornev a decade ago [32]. In the framework of model (1), he studied qualitatively propagation of planar waves through a border dividing the medium into two half-planes with different diffusion coefficients ($D_{1,2}$) and identical local kinetics. Considering incident and refracted waves as being planar waves and using conditions of continuity for concentration variables and diffusion fluxes, he reached the following conclusions:

(1) Autowaves undergo refraction at angles uniquely determined by the diffusivities of the homogeneous regions. That is, the initial position of autowave fronts on both sides of the D-jump line can be preset arbitrarily, but, as time elapses, incident and refracted angles become entirely determined by diffusion

$$\sin\psi_{\text{incid}} = \sqrt{D_1/(D_1+D_2)}, \quad \sin\psi_{\text{refr}} = \sqrt{D_2/(D_1+D_2)}, \tag{5}$$

and obey an opticslike sin condition

$$\frac{\sin\psi_{\text{incid}}}{\sin\psi_{\text{refr}}} = \sqrt{D_1/D_2} \equiv n_{12}, \tag{6}$$

(2) ''In active media with diffusion, reflected waves are not observable. . . . In optics, the total internal reflection takes place when the angles of incidence exceed Brewster's angle. This phenomenon is not observed in active media; the refracted component of the autowave . . . exists with any value of ψ_{incid} within the interval $0<\psi_{\text{incid}}<\pi/2$'' [33].

(3) When an autowave front travels from a region with a small value of D to a region with a bigger one, and the ''refractive index'' n_{12} is less than a certain critical value, the front cannot pass across the interface: the line of D jump becomes opaque for approaching plane autowaves.

Mornev's simplified analysis was based on a straightforward generalization of one-dimensional propagation for 2D EM. One of the main features of autowave propagation in 2D and 3D cases, namely, the curvature effect, was not taken into account. As a result, a nonphysical singularity of the autowave front on the line of D jump appears. Also, he did not consider inhomogeneity due to variation of nonlinear kinetics, which would allow for comparison with recent experiments [12,16].

In this paper we study the evolution of autowave fronts in 2D EM containing one straight semipenetrable boundary between two areas with different properties. Our study is based on the kinematic approach, a brief description of which is given in Sec. II. In Sec. III we construct steady-state wavefront configurations in an unbounded medium consisting of two adjacent half-planes with different properties. Next we introduce one impenetrable boundary (a half-plane with an adjacent stripe) and then two impenetrable boundaries (two adjacent strips with different properties). We explore variations in both diffusion coefficients and reaction rates. In Secs. IV and V we compare our results with recent experiments and discuss further implications of our findings.

II. MODEL AND SOLUTIONS

A comprehensive consideration of autowave propagation in piecewise media has to be based on system (1). Unfortunately, analytical solutions for 2D reaction-diffusion systems are not available. Numerical integration is useful in many cases but can be extremely demanding of computer resources. Therefore some preliminary analytical or approximate results are advisable before one starts ''number crunching.'' In order to get an idea of what to expect, we face this study on the kinematic approach—the only method giving a global, though certainly approximate, picture of the phenomena under consideration. Here we mention those details of the approach which are necessary for understanding our results, referring for a fuller treatment to recent reviews [34].

In the kinematic description a pulse structure is reduced to

one point, so that an excited region in a 2D EM is conceived as an infinitely thin curved line with a normal vector pointing in the direction of the excitation propagation. Each point on the linelike front moves in the normal direction with a velocity $V=V(k)$ determined by the front curvature k at this point. For reaction-diffusion systems this dependence, for k not too close to some critical value k_{cr}, can be taken as linear [6,8,9]

$$V(k)=V_0-Dk \quad \text{(eikonal approximation)}. \tag{7}$$

Here V_0 is the velocity of the planar front, and D is the diffusion coefficient of the excitation variable. The kinematic approach specifies the shape of the wave front by the intrinsic equation $k=k(l,t)$ that for each moment of time t relates the curvature of the front to the arc length along the front l. For a steady-state front (which propagates without change of shape) $\partial k/\partial t=0$, and the profile of an endless front, $l\in(-\infty,+\infty)$, propagating in 2D flat EM obeys the following nonlocal integro-differential equation [35]

$$k(l)\int_0^l k(\xi)V[k(\xi)]d\xi+\frac{dV[k(l)]}{dl}=0. \tag{8}$$

By putting the right-hand side equal to zero we have excluded from consideration circulating solutions, which are irrelevant to the present work [36]. A boundary condition $k(0)$ also has to be specified in order to determine a unique solution of Eq. (8).

The intrinsic equation $k(l)$ defines the front curve uniquely except for its position and orientation on a plane. Parametric representation of an actual front line in the Cartesian frame of reference can be constructed from the intrinsic equation by a standard procedure [25,37]. In particular, the angle between the tangent to the wave front at the point l and the axis OY, taken as positive if measured clockwise from the positive direction of the axis OY, is

$$\theta(l)=-\int_0^l k(\xi)d\xi. \tag{9}$$

Multiplying (8) by $V(k)$, integrating once, and changing variables from l to θ, we find that

$$\left[\int_0^\theta V(\theta)d\theta\right]^2+[V(\theta)]^2=[V(0)]^2, \tag{10}$$

where $V(0)$ denotes the normal velocity of the wave at $\theta=l=0$, to be distinguished from V_0, the velocity at $k=0$. Equation (10) has the obvious solution

$$V(\theta)=V(0)\cos\theta, \tag{11}$$

which implies that the wave propagates along the X axis with speed $V(0)$. Differentiating (11) with respect to l, we find that

$$D\frac{dk}{dl}+k\sqrt{[V(0)]^2-[V(k)]^2}=0. \tag{12}$$

Solutions of this first-order differential equation are parametrized by the value $k(0)$ [25].

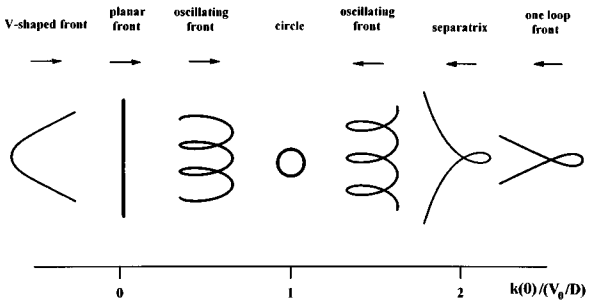

FIG. 1. Shapes of the fronts corresponding to the steady-state solutions of the kinematic model [Eq. (8)] in the eikonal approximation. The arrows show the propagation direction of patterns. In all cases $V_0/D=1$. Qualitative features of the solutions are discussed in the text.

A planar front $[k(l)=0]$ propagating with constant velocity $V(k)=V_0=\text{const}$ is obviously a trivial steady-state solution of (12) and hence (8).

For $k(0)<0$, the front propagates in the form of a V-shaped wave [38]. Its profile is described by the soliton-type expression

$$k(l)=-\frac{1}{D}\frac{[V(0)]^2-V_0^2}{V_0+V(0)\cosh\left[\dfrac{l}{l_0}\right]}, \quad -\infty<l<\infty, \tag{13}$$

with the characteristic length $l_0=D/\sqrt{|[V(0)]^2-V_0^2|}$. The curvature of this front decreases exponentially as l goes to infinity $k(l\to\pm\infty)\to 0$ and the asymptotic angle follows directly from Eq. (11), $\theta(l\to\pm\infty)=\arccos[V_0/V(0)]$. The V-shaped pattern moves uniformly, with velocity $V(0)>V_0$ (i.e., faster than a planar front), from left to right as shown in Fig. 1. As $k(0)\to 0$, the angle between asymptotes of a V-shaped wave increases to π and the velocity of the pattern decreases to V_0, that is the pattern converts into a plane wave.

Positive $k(0)$ gives birth to space oscillating fronts with shapes described by

$$k(l)=-\frac{1}{D}\frac{[V(0)]^2-V_0^2}{V_0+V(0)\cos\left[\dfrac{l}{l_0}\right]}. \tag{14}$$

As $k(0)$ increases from zero up to $k(0)\simeq V_0/D$, the amplitude of the front oscillations decreases from V_0/D to zero, and period decreases from infinity to $2\pi D/V_0$. The front in this case propagates with a speed $V(0)<V_0$, from the left to the right as depicted in Fig. 1. At $k(0)=V_0/D$ the front degenerates in a nonpropagating ring of radius $1/k=D/V_0$. When $k(0)$ becomes greater than V_0/D and moves toward $2V_0/D$ the space oscillating front appears again but now the behavior of its amplitude and period is opposite to that which took place when $k(0)$ ran from zero to V_0/D. Also the direction of front propagation reverses: the front moves from the right to the left in Fig. 1 with the speed $|V(0)|<V_0$.

The value $k(0)=2V_0/D$ corresponds to the separatrix solution which has the algebraic soliton-type shape

$$k(l)=\frac{2V_0/D}{1+\left(\frac{l}{D/V_0}\right)^2}. \tag{15}$$

The corresponding front retains only one loop, with asymptotically flat wings, $k(l\rightarrow\pm\infty)\rightarrow 0$, separated by an angle of π. The front moves with a speed V_0, from the right to the left (see Fig. 1).

Further increase of $k(0)$ beyond $2V_0/D$ retains the one-loop structure of the front [Eq. (13)] but changes the asymptotic angle α between the wings, which now becomes smaller than π and goes to zero as $k(0)\rightarrow\infty$. The front still moves from the right to the left, now with the velocity $|V(0)|>V_0$.

Linear stability analysis shows [25] that the solutions are stable with respect to small localized perturbations which disappear diffusively (with characteristic time D/V_0^2), traveling along the front towards the regions of maximum curvature. Nonlocalized (even small amplitude) perturbation may lead to the formation of a pattern with new parameters.

Stable V-shaped waves have been observed recently in the BZ reaction and in numerical experiments with the Oregonator model [39,40]. The other solutions are self-crossing and therefore cannot be identified with any stationary autowave pattern in homogeneous EM. The looping structure of these solutions is an artifact of our extrapolation of the linear dependence Eq. (7) beyond the critical curvature $k_{\rm cr}$, where continuous propagating fronts do not exist. Incorporating critical curvature into the theory destroys loops, converting them into cusps [41], but does not essentially change the regular parts of the solutions. Therefore these regular parts (parts which have curvature less then $k_{\rm cr}$) can be used for describing patterns in piecewise stratified EM, that is, EM consisting of stripes with semipenetrable and impenetrable straight-line borders between them. The situation here is similar, for instance, to that in classical electrodynamics, when one is evaluating the electric field of a uniformly charged infinite cylinder (conductor). Both solutions of Poisson's equation for the potential are singular (one in the origin, the other at infinity) and, hence, are unphysical in homogeneous media. But when applied to a piecewise constant problem, being appropriately concatenated at the boundary of the property jump, they form a bounded solution since only their regular parts are used [42].

III. UNBOUNDED MEDIA

Boundary conditions for ''reactants'' in the original system (1) translate into geometric constraints on the wave-front line [3,4,13,25,26,43]. No-flux (impenetrable) boundary conditions (2) imply, in terms of the kinematic model, that a steady-state front must propagate so that its line always meets the boundary orthogonally. If the boundary is flat the simplest example is a plane front propagating parallel to the boundary (i.e., the front line is perpendicular to the impenetrable boundary). Another possibility appears if we recall that a V-shaped wave propagating along the axis OX remains perpendicular to the line of its symmetry (axis OX) at any moment of time. Thus, if we replace one half-space, say $y<0$ (see Fig. 1), with an impenetrable border, the rest of the V-shaped wave in the upper half-space ($y>0$) will remain unperturbed. Hence a half piece of the V-shaped wave describes a ''planar'' autowave front tilted at the angle $\theta(l\rightarrow\infty)$ and steadily propagating along the straight-line impenetrable boundary. Note, that the velocity of this front along the boundary is higher, $V(0)=[V_0/\cos\theta(l\rightarrow\infty)]$, than the propagation velocity of an infinite planar front because of the ''scissors'' effect. A plane wave and a half piece of V-shaped wave constitute the only steady-state configurations possible in 2D EM occupying a half-plane.

For a semipenetrable boundary, fronts must pass smoothly through lines of discontinuity. In terms of the kinematic approach, the angle θ [see Eq. (9)] must be a continuous function across the semipenetrable boundary or, as follows from Eq. (11), projections of the normal front velocity [$V(0)$] have to be identical on both sides of the discontinuity line. Notice that the front curvature may have a discontinuity at the boundary.

A. Piecewise change in excitability

Let us consider a flat 2D EM occupying the whole plane. We characterize the medium by its macroscopic parameters: the planar front velocity V_0 and the diffusion coefficient D. We suppose also that in the upper half-plane ($y>0$) excitability is greater than in the lower half-plane ($y<0$), i.e., the planar front velocity in the upper half-plane is greater than the velocity in the lower half-plane: $(V_0)_{\rm up}>(V_0)_{\rm low}$. The diffusion coefficient we suppose to be the same in both half-planes. Such conditions can be generated, for instance, in a light-sensitive BZ system by the technique developed in [13] or by making use of the oxygen inhibition of excitability in the ferroin-catalyzed BZ reaction [12]. We suppose that the transition region between areas with different excitability is infinitely thin and, hence, the medium can be considered as piecewise constant. The assumptions closely approximate experimental conditions [4,12,13].

If we start with an infinitely extended planar autowave front having some arbitrary angle to the OX axis, how will it evolve in time? Obviously, the shape of the front must change in the course of its evolution because local velocity is different for different parts of the front line: the part in the lower half-plane will lag compared to the part in the upper area. If the difference of velocities is not very large, the front will remain continuous (will not break at the line of discontinuity) but will curve, relaxing to a steady-state configuration where any point of the front must move along the axis OX with the same velocity $V(0)$. Two factors will contribute to the process of velocity equalization on both sides of the semipenetrable boundary: ''scissors'' and curvature effects. The shape of the resulting steady-state profile will also depend on initial conditions, in our case on the initial angle between the front and the boundary. The detailed evolution of a front to its asymptotic (steady-state) configuration in EM with a discontinuity is the subject for a future paper. Here we construct asymptotic (in time) steady-state front configurations and describe relaxation processes only qualitatively.

Let us suppose first that at the initial moment of time ($t=0$) a planar autowave front propagating in the positive direction along the axis OX makes an acute angle with the boundary line, as depicted in Fig. 2(a), therefore $0<[\theta_0\equiv\theta(t=0)]<\pi/2$. At the next moment of time the part of the front in the upper half-plane will pass over its

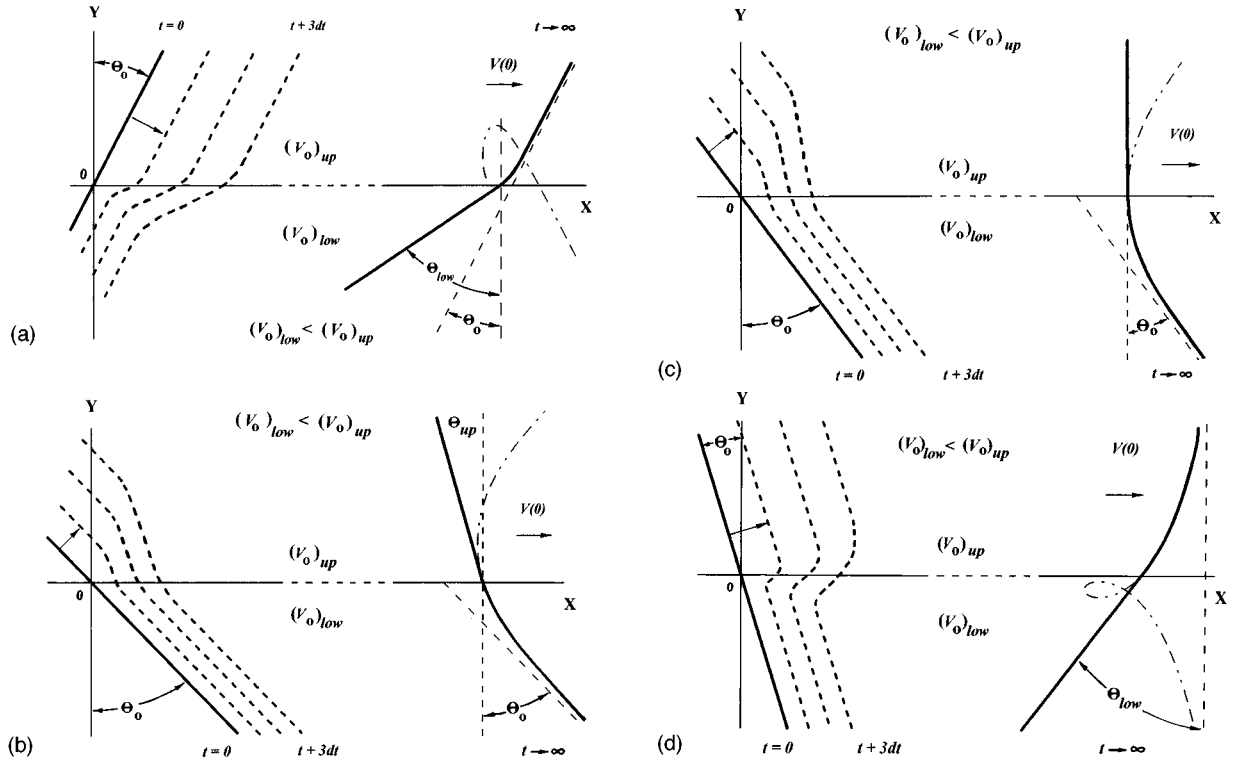

FIG. 2. Time evolution of the initially plane wave front in an EM consisting of two half-planes with different excitability. The semipenetrable boundary is located at $y=0$. The plane front velocity in the upper half-plane is higher than in the lower half-plane: $(V_0)_{\rm low}<(V_0)_{\rm up}$. The front moves from left to right. The initial state and the final steady-state are depicted by thick solid lines. Three intermediate front configurations are drawn by thick dashed lines. The double-dotted double-dashed line shows the fragment of the corresponding homogeneous pattern used for constructing the front line in a given piecewise medium. (a) the initially plane front has an acute angle with the boundary line ($0<\theta_0<[\pi/2]$); (b) the initially plane front has an obtuse angle with the boundary line ($-(\pi/2)<\theta_0<\theta_{\rm cr}<0$); (c) the initially plane front intersects the boundary line at the critical angle ($\theta_0=\theta_{\rm cr}$); (d) the initially plane front intersects the boundary line at an angle larger than critical ($\theta_{\rm cr}<\theta_0<0$).

counterpart in the lower half-plane. Since diffusion keeps a front line smooth, the upper and lower parts of the front turn to be connected in the transient preboundary region with a curved kinklike fragment which meets the boundary at an angle larger than θ_0. Distant regions of the front on both sides of the boundary will remain unperturbed. At subsequent times the ''kink'' will spread out, smoothing the front branch in the upper half-plane, without changing its asymptotic angle $[\theta(t\to\infty,l\to\infty)=\theta_0]$, and reswitching the front branch in the lower half-plane from a plane front with initial angle θ_0 to a plane front with final angle $\theta_{\rm low}$. The steady-state configuration which the front achieves when $t\to\infty$ can be constructed in this case from the solution (13) (at $k>0$), which is asymptotically flat and tilted at the angle θ_0, for the upper part, smoothly matching a tilted planar front for the lower part. The relationship between angles θ_0 and $\theta_{\rm low}$ arises from the requirement that the final steady-state front propagates along the axis OX with the same velocity in the lower half-plane $V(0)=[(V_0)_{\rm low}/\cos\theta_{\rm low}]$ as in the upper half-plane $V(0)=[(V_0)_{\rm up}/\cos\theta_0]$. Hence

$$\cos\theta_{\rm low}=\frac{(V_0)_{\rm low}}{(V_0)_{\rm up}}\cos\theta_0. \tag{16}$$

Note that, though the front line of the pattern is smooth, the curvature of the front undergoes a jump at the semipenetrable boundary. Since the value of the ratio $[(V_0)_{\rm low}/(V_0)_{\rm up}]$ is less then unity, Eq. (16) can be solved for $\theta_{\rm low}$ for any $\theta_0\in(0,\pi/2)$, so the steady-state pattern in this case is similar to Fig. 2(a) for any initial angles $\theta_0\in(0,\pi/2)$.

Next we consider the case when the initial planar front makes an obtuse angle with the boundary line ($\theta_0<0$) and is bounded away from zero ($0<\cos\theta_0<[(V_0)_{\rm low}/(V_0)_{\rm up}]$, see Fig. 2(b)). In the process of evolution, the part of the front in the lower half-plane will lag the part in the upper half-plane, which will generate a negatively curved region on the front in the vicinity of the boundary. The perturbation in the upper half-plane will propagate along the front, away from the boundary, converting this part into a planar front with an angle $\theta_{\rm up}$ different enough from θ_0, appropriate to compensate for the velocity difference in the upper and lower half-planes. The lower branch of the front will be disturbed only in a vicinity of the boundary becoming a portion of the V-shaped wave [solution (13) at $k<0$] with the asymptotic angle $\theta_{\rm low}(t\to\infty,l\to\infty)=\theta_0$. Equating the propagation velocities of the resulting pattern determined from its upper portion $V(0)=[(V_0)_{\rm up}/\cos\theta_{\rm up}]$ and from a distant portion of the lower branch $V(0)=[(V_0)_{\rm low}/\cos\theta_0]$ we find that

$$\cos\theta_{\rm up}=\frac{(V_0)_{\rm up}}{(V_0)_{\rm low}}\cos\theta_0. \tag{17}$$

As long as $\cos\theta_0 < [(V_0)_{\rm low}/(V_0)_{\rm up}]$, this equation for $\theta_{\rm up}$ has a solution. The smoothly matching boundary condition means $\theta_{\rm up}=\theta_{\rm low}$ $(l=0)$.

Now, at given $(V_0)_{\rm up}$ and $(V_0)_{\rm low}$, let us increase the initial angle the planar front makes with the boundary line (make θ_0 closer to zero). At some moment we will approach the condition

$$\frac{(V_0)_{\rm low}}{(V_0)_{\rm up}}=\cos\theta_0, \tag{18}$$

which, taking into account (17), gives $\theta_{\rm up}=0$, and, hence, $\theta_{\rm low}(t\to\infty, l=0)=0$. This angle may be called the critical angle

$$\theta_0=\theta_{\rm cr}=\arccos\left[\frac{(V_0)_{\rm low}}{(V_0)_{\rm up}}\right].$$

In this situation the front in the lower half-plane is exactly a half of the *V*-shaped wave, and the planar front in the upper half-plane becomes orthogonal to the boundary [see Fig. 2(c)]. Hence the pattern propagates with the velocity $V(0)=(V_0)_{\rm up}$. The jump in curvature at the boundary is given in this case by the simple expression

$$k_{\rm up}(l=0)-k_{\rm low}(l=0)=\frac{(V_0)_{\rm up}-(V_0)_{\rm low}}{D}. \tag{19}$$

Further increasing θ_0 toward 0 would make (17) unsolvable because the right-hand side would become greater than unity. For these initial conditions, the steady-state configuration is qualitatively different from the combination of *V*-shaped and planar waves we have just described. In order to equalize velocities, while maintaining a smooth concatenation with the front part in the upper half-plane, the part of the front in the lower half-plane will have to change the sign of its tilt angle [see Fig. 2(d)]. The front line consists of a piece of a tilted planar front, this time in the lower half-plane, matching smoothly a piece of the one-loop solution (15) in the upper half-plane. Since the latter solution becomes flat at $l\to\infty$ $(y\to\infty)$ and oriented perpendicular to the boundary line, the pattern propagation velocity is $V(0)=(V_0)_{\rm up}$. This defines the tilting angle of the front in the lower half-plane

$$\cos\theta_{\rm low}=\frac{(V_0)_{\rm low}}{(V_0)_{\rm up}}. \tag{20}$$

Note that, within the region of applicability of (20), the angle $\theta_{\rm low}$ does not depend on the initial angle θ_0: the pattern in Fig. 2(d) holds for any θ_0 in the region $[(V_0)_{\rm low}/(V_0)_{\rm up}]<\cos\theta_0\leqslant 1$. The geometrical stability of the patterns we have constructed follows from the stability of the solutions from which these patterns have been built [25,40].

B. Piecewise diffusivity

Now we consider the case when the reaction rate in both half-planes is identical but the diffusivity is different: $D_{\rm up}\neq D_{\rm low}$. Experimentalists create such discontinuities using polyacrylamide or silica gel (including their combinations with aqueous solutions) [29,44] or porous glasses [45]. Variation of the diffusion coefficient not only regulates the curvature effect [see Eq. (7)] but induces a variation of the plane-front velocity V_0 as well because $V_0\sim\sqrt{D}$ [3]. Because of the square root dependency, the variation of D cannot just be scaled out even in the eikonal approximation we use here. We can construct steady-state front configurations as above, and the resulting patterns differ only quantitatively from the previous subsection. The critical angle this time is given by the expression $\theta_{\rm cr}=\arccos(\sqrt{D_{\rm low}/D_{\rm up}})$, and in corresponding expressions connecting final front angles on the two sides of the discontinuity line the ratio $(V_0)_{\rm low}/(V_0)_{\rm up}$ has to be replaced by the ratio $\sqrt{D_{\rm low}/D_{\rm up}}$. The general case, in which both excitability and diffusivity vary, does not introduce any qualitatively new features.

IV. BOUNDED MEDIA

A. Half-plane with a stripe

Here we consider wave-front dynamics in 2D EM occupying a half space $y>0$ with a stripe (of width *W* adjacent to the axis *OX*) where excitability is different from the upper half-plane. The line $y=0$ constitutes the semipenetrable boundary while the line $y=-W$ is the impenetrable boundary. This ''preboundary'' layer can be taken as a first approximation to the situation where an impenetrable boundary introduces inhomogeneity only in a narrow layer adjacent to the boundary, while the rest of the medium remains homogeneous. In the beginning of the preceding section we pointed out two steady-state configurations existing in a half space, a planar wave and half of a *V*-shaped wave, that would be possible in the absence of the semipenetrable boundary. What kind of steady-state front configurations can we construct after introducing the semipenetrable boundary?

This time, due to the explicit asymmetry, we have to distinguish whether excitability is higher in the stripe or in the rest of the EM. To start, let the excitability be lower in the stripe, which makes the velocity of planar front here $(V_0)_{\rm low}$ lower than in the outside area: $(V_0)_{\rm low}<(V_0)_{\rm up}$. Grant initially a planar front which makes an acute angle with the boundary lines $(0<\theta_0<\pi/2)$. Since the steady-state front must be orthogonal to the impenetrable boundary, the lower branch of the pattern has to be a piece of the *V*-wave solution (13), which would match the upper branch smoothly and approach the impenetrable boundary at a right angle. The upper fragment of the front will be either a branch of the one-loop solution (13), if the initial angle is acute $(0<\theta_0<\pi/2)$, or a branch of the algebraic soliton solution (15) if the initial angle is right $(\theta_0=0)$ or even obtuse $(-\pi/2<\theta_0<0)$. The resulting steady-state front configurations are depicted in Figs. 3(a), 3(b), 3(c). The velocity of the pattern resulting from the initial conditions $0<\theta_0<\pi/2$ is $V(0)=[(V_0)_{\rm up}/\cos\theta_0]$ and from the initial angle $-\pi/2<\theta_0\leqslant 0$ is $V(0)=(V_0)_{\rm up}$. Neither velocity depends on the stripe width. The curvature of the front at the impenetrable boundary then is

$$k_{\rm low}(l=0)=\frac{(V_0)_{\rm low}-(V_0)_{\rm up}/\cos\theta_0}{D}, \tag{21}$$

and also does not depend on the stripe width. The concatenation angle (the angle the steady-state front makes with the

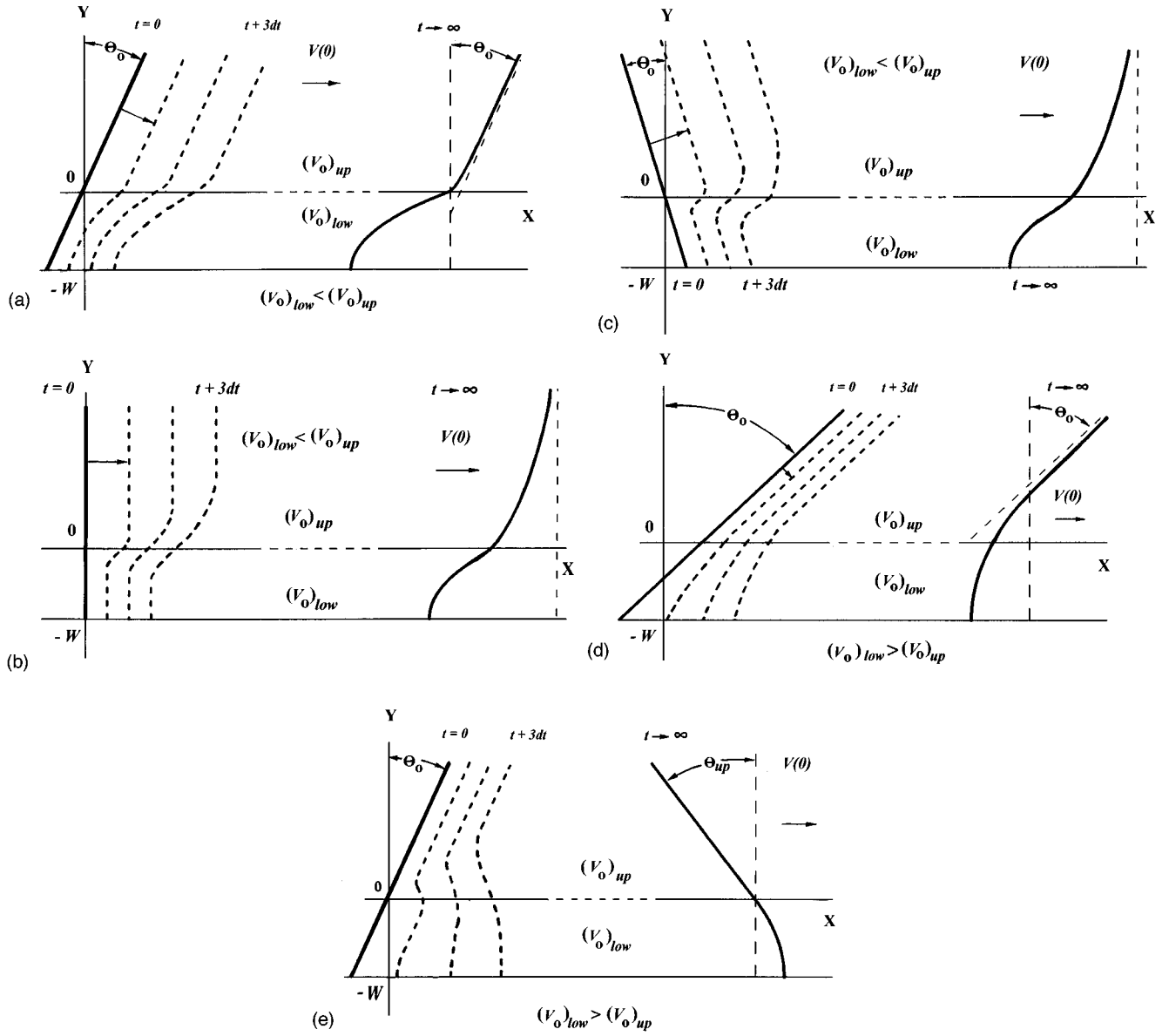

FIG. 3. Time evolution of an initially plane wave front in an EM occupying a half-space $y>0$ with a preboundary layer of width W where the excitability is different. The semipenetrable and impenetrable boundaries are located at $y=0$ and $y=-W$, respectively. The initial state and the final steady state are depicted by thick solid lines. Three intermediate front configurations are shown by thick dashed lines. (a) excitability is lower in the preboundary layer, and the initially plane front makes an acute angle with the boundaries ($0<\theta_0<[\pi/2]$); (b) as in (a) except $\theta_0=0$; (c) as in (a) except $-[\pi/2]<\theta_0<0$; (d) excitability is higher in the preboundary layer and $\theta_{cr}<\theta_0<(\pi/2)$; (e) as in (d) except $0<\theta_0<\theta_{cr}$.

semipenetrable boundary) $\theta_{low}(0)=\theta_{up}(0)$ can be determined using Eqs. (9), (13), (15), and is, certainly, dependent on the stripe width. These patterns are, in fact, exactly half pieces of the bell-like waves in the EM with a stripe discussed in [26].

Notice that, in contrast to unbounded media, this time the critical angle does not appear. The regime analogous to Fig. 2(b) does not exist in a medium with a stripe.

Next consider the situation where excitability and hence planar front velocity is higher in the stripe than in the upper half-plane. Again, we start from an acute initial angle between the front line and the boundary ($0<\theta_0<\pi/2$). The analogous configuration in an unbounded medium is in Fig. 2(b) but now the upper half-plane is replaced with a stripe of finite width. Let θ_0 be large enough: $\cos\theta_0<[(V_0)_{up}/(V_0)_{low}]$. The impenetrable boundary will change only slightly the upper branch of the steady-state pattern in Fig. 2(b), converting it into a fragment of a V-shaped wave with its top on the impenetrable boundary and matching smoothly the front fragment outside the stripe, which is a fragment of a V-wave too [see Fig. 3(d)]. The asymptotic angle of the outside branch remains equal to the initial angle θ_0. The curvature of the front at the impenetrable boundary, determined from the condition that the steady-state front must have the same propagation velocity in the stripe $[V_{low}(0)=(V_0)_{low}-D\cdot k_{low}(0)]$ as outside

$$\left[V_{up}(l\to\infty)=\frac{(V_0)_{up}}{\cos\theta_0}\right],$$

is given again by Eq. (21). The connection between the concatenation angle and the stripe width W can be made using Eqs. (9), (13).

For the limiting case, when $\cos\theta_0=(V_0)_{\rm up}/(V_0)_{\rm low}$, the outside part of the front becomes exactly half of a V wave while the front in the stripe becomes a piece of a plane wave. The propagation velocity of the pattern in this case coincides with the velocity of the planar front in the stripe.

When the initial angle θ_0 becomes enough, $\cos\theta_0>(V_0)_{\rm up}/(V_0)_{\rm low}$, the initial front undergoes transformations similar to those depicted in Fig. 2(d). This time the front inside the stripe will significantly overpass its counterpart outside and, in order to be orthogonal to the impenetrable boundary and smoothly match the upper branch, becomes convex in the direction of its propagation, constituting a piece of the oscillating solution (14). The front in the outside area becomes converted into a planar front tilted opposite to its initial inclination. The resulting steady-state configuration is depicted in Fig. 3(e). The concatenation angle is equal to the external branch tilting angle $\theta_{\rm up}=\theta_{\rm low}(l^*)=-\int_0^{l^*}k_{\rm low}(\xi)d\xi=\theta_{\rm up}[l^*,V(0),(V_0)_{\rm low},D]$ and the stripe width can be related to the pattern fragment in the stripe as $W=\int_0^{l^*}\cos\theta_{\rm low}(\xi)d\xi$ [25]. The propagation velocity of the pattern is $V(0)=(V_0)_{\rm up}/\cos\theta_{\rm up}$. Using these equations, one can express $\theta_{\rm up}$ and $V(0)$ as functions of D, $(V_0)_{\rm up}$, $(V_0)_{\rm low}$, W. Thus, this time, the pattern propagation velocity depends on the stripe width, as does the final front tilting angle in the upper half space. Further decreasing θ_0 and even going to negative θ_0 (obtuse angle between the initial front line and boundary) will not change the qualitative character of the resulting steady-state pattern. In fact, the configuration discussed here is just half of the pattern observed recently in unbounded BZ EM with a stripe [13] and discussed in [25]. Therefore, the dependence of pattern velocity on stripe width derived there holds for the case discussed here: the pattern velocity $V(0)$ is a monotonically increasing function of stripe width W and runs from $(V_0)_{\rm up}$, for $W=0$, up to $(V_0)_{\rm low}$, for $W\to\infty$. Furthermore $\theta_{\rm up}$ is a monotonically decreasing function of $W(\theta_{\rm up}<0)$, running from 0 for $W=0$ up to the value determined by the critical angle in an unbounded medium [see Eq. (20)] for $W\to\infty$.

B. Stripe divided by a semipenetrable boundary

In this subsection we consider a stripe of EM (the medium confined between two parallel impenetrable boundaries) divided along its length by a semipenetrable boundary. In other words, the medium consists of two adjacent stripes of widths W (for $y<0$) and L (for $y>0$) with different excitability. Without loss of generality we may choose the lower stripe as less excitable: $(V_0)_{\rm low}<(V_0)_{\rm up}$. This time only a combination of V-shaped and oscillating solutions (Fig. 4) can give us a front which is orthogonal to the impenetrable boundaries $[\theta_{\rm up}(y=L)=\theta_{\rm low}(y=-W)=0]$ and is smooth at the semipenetrable boundary $[\theta_{\rm up}(y=0)=\theta_{\rm low}(y=0)]$. In the upper part, the front is convex, which reduces its propagation velocity $V(y=L)$ compared to $(V_0)_{\rm up}$. In the lower strip the front is concave (a fragment of a V-shaped wave), which enhance its propagation velocity $V(y=-W)$ compared to $(V_0)_{\rm low}$. The steady-state pattern in this case is half of the bell-like wave observed recently in experiments with BZ reaction [13] and described in [25]. It has been shown in [25] that the propagation velocity of such a pattern is a monotonic function of the stripe width, decreasing with the increase of W and increasing with the increase of L.

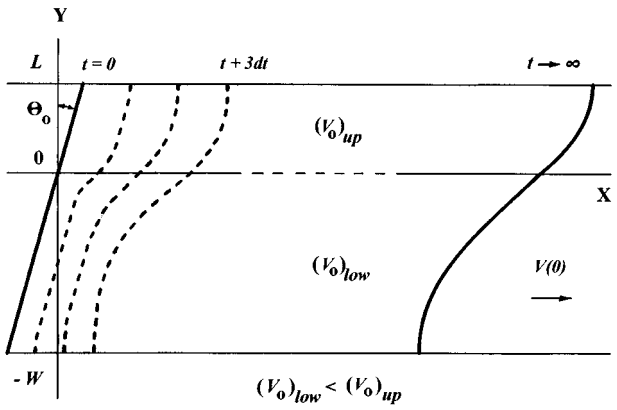

FIG. 4. The evolution of an autowave front in a stripe of EM divided along its length by a semipenetrable boundary. The initial state and final steady state are depicted by thick solid lines. Three intermediate front configurations are shown by thick dashed lines.

V. DISCUSSION

For autowaves the excitation zone is followed by a refractory zone which does not allow for immediate back propagation of excitation. For this reason autowaves annihilate in collision with each other and die at impenetrable boundary. Reflection of an excitation pulse from an impenetrable boundary has never been observed, but several theoretical works indicate its possibility in the cubic autocatalysis model [30] and in a BZ model close to a subcritical Hopf bifurcation [31]. Concerning a semipenetrable boundary, delayed reflection in a nerve fiber has been shown to exist if the duration of excitation in the medium behind the boundary is larger that the refractory time in the medium in front of the boundary [46].

In 2D EM an oblique collision is possible, which introduces a geometrical component to the colliding and ''scattered'' fronts. No rigorous theoretical PDE study of oblique waves propagating through a discontinuity line has been accomplished for 2D EM so far, and experimental data are very limited [12,29], but we have shown that some insight into the geometry of collisions can be gained from purely kinematic considerations. In comparing our findings with available experimental and theoretical data, we consider only oblique collisions and assume that wave-boundary interactions do not change the dynamics of excitation-recovery variables so much as to allow for back propagation (reflection in 1D).

Generally speaking, to observe refraction and reflection, we would like to generate as an initial condition a piece of plane wave propagating toward a line of discontinuity in the medium. But for autowaves in EM this initial state is not suitable because the free ends of the plane wave would curl up into spiral sources, which would greatly complicate the interpretation of the results. To avoid this problem we start from an infinitely extended planar front propagating at an oblique angle to the boundary. The part of the initial front

that is moving toward the boundary we consider as the incident wave. The initial part moving away from the boundary prevents spirals from forming as it sweeps off to infinity. We ignore this part, following instead the evolution of the incident wave as it moves into and interacts with the boundary. We observe that either the incident wave will pass through the boundary and propagate away at a characteristic angle of refraction, or if the angle of incidence is sufficiently shallow, the wave will suffer total internal reflection. Notice that an autowave always passes smoothly through a semipenetrable boundary. Hence the angle at which the wave front meets the boundaries is always equal to the angle at which it leaves the boundary, although the front is generally curved as it passes through the neighborhood of the boundary. Further from the boundary the fronts approach asymptotically to constant direction of propagation, which allows us to define unambiguously angle of refraction and reflection.

Let us take a look first at Figs. 2(a), 2(b) which correspond to autowaves propagating (using optical terminology) from less ''dense'' (more excitable) to more ''dense'' (less excitable) medium [Fig. 2(a)], and in the opposite direction [Fig. 2(b)]. In both cases the incident wave [the upper half-plane in Fig. 2(a) and the lower half-plane in Fig. 2(b)] retains its angle asymptotically: $\theta(t\to\infty, l\to\infty)=\theta_0$. The angle of the refracted wave differs from the initial angle θ_0 and is determined by the property difference across the boundary. From Eqs. (16) and (17), taking into account that the ray angle ψ used in optics is related to our front angle θ as $\psi=(\pi/2)-\theta$, it follows that incident and refracted angles obey the opticlike Snell's law $(\sin\psi_{\text{incid}}/\sin\psi_{\text{refr}})=n'$, where the relative index of refraction is $n'=[(V_0)_{\text{up}}/(V_0)_{\text{low}}]$ or (for different diffusion and identical kinetics) $n'=\sqrt{D_{\text{up}}/D_{\text{low}}}$. Experimentally observed values for refractive indexes in chemical excitable systems are: $n'\sim 1$ to 2.5 for the light-sensitive BZ reaction [12,13,47], $n'\sim 1.2$ for the solution-gel system [29], or $n'\sim 3.7$ for the solution-porous glass system [45]. By comparison the highest known value for the refractive index in optics $n'\approx 2.5$ to 3.5 [10,48]. For a reaction-diffusion PDE system like FHN, the value of the ratio $(V_0)_{\text{up}}/(V_0)_{\text{low}}$ can be arbitrarily large but in computer simulations this ratio, with reasonable expenses of computer resources, can only be a several fold [49]. Although fronts in Figs. 2(a), 2(b) are curved near the boundary in different ways, the principle of reversibility holds for asymptotic angles: the incident angle in Fig. 2(a) is equal to the refracted angle in Fig. 2(b). In neither case do we observe wave reflection.

Our theory agrees with Mornev's predictions [32] concerning the validity of Snell's law and the value for the refractive index, but does not confirm his conclusion that both incident and refracted angles are determined by the medium properties on the two sides of the discontinuity line. In our theory the asymptotic angle of the incident wave cannot be changed in the process of the wave-boundary collision, and this angle defines uniquely, through Eqs. (16), (17), the angle of the refracted wave. Mornev's mistake lies in neglecting the autowave curvature effect essential for any consideration of autowave propagation in 2D EM.

The only known experimental study of autowave refraction has been done by Zhabotinsky, Eager, and Epstein [12,16], who studied wave propagation in the ferroin-catalyzed BZ EM using oxygen inhibition of excitability to create a sharp boundary between two regions with different wave velocities. Although they claimed to have confirmed Snell's law for autowaves, the interpretation of their observations seems problematical to us. The initial wave was initiated in those experiments by a pointlike source placed on the semipenetrable boundary. In homogeneous medium it would produce a target pattern (expanding circular wave) which now is distorted by the inhomogeneity of the medium. Our concern is that a target pattern is not a plane wave. Therefore, they cannot measure the asymptotic angles at which the plane waves are propagating: these are the incident and refracted angles needed to test Snell's law. Since the curvature of the front changes continuously in the two regions and across the boundary, it is always possible to find two points on the front lying on different sides of the boundary for which tangents to the front will define angles that satisfy Snell's law.

In the only experimental paper about 2D autowave refraction in a medium with piecewise change in diffusion, refraction of autowaves has been observed qualitatively but the conditions of the experiment did not allow for quantitative measurements [29].

When a wave propagates from less excitable to more excitable medium and the initial angle θ_0 exceeds a critical value [see Fig. 2(d)], the slope of the initial (incident) wave changes, in the process of wave-boundary interaction, so that the final wave front is propagating away from the boundary, which means that the incident wave is reflected by the boundary. A refracted component (a wave propagating in the upper half-plane away from the boundary) is absent in this case. Reflection for initial angles larger or equal to the critical angle is known in optics as total internal reflection [10]. Thus, in our model, autowaves do not undergo reflection in general but only total internal reflection. In contrast to optics, the angle of this reflected wave is uniquely determined by the ratio $(V_0)_{\text{up}}/(V_0)_{\text{low}}$ and does not depend on the incident angle, as long as it is larger than the critical angle. For total internal reflection in optics, the wave in the target medium propagates in the direction parallel to the discontinuity line [10]. This is similar to our finding for autowaves [Fig. 2(d), upper half-plane]. Being totally reflected, light penetrates a target medium only to a depth of a few wave lengths. The width of the target medium is crucially important in optics only when it becomes comparable to the wave length of the light, which, in fact, destroys the phenomenon of total internal reflection. Our study of a medium with a stripe (Sec. IV) shows the influence of medium size on the phenomenon of total internal reflection for autowaves. When the plane wave hits the boundary from the restricted area (stripe) and the target medium is unrestricted [see Fig. 3(b), 3(c)], it turns out always to be in the condition of total internal reflection: the final steady-state branch in the stripe always moves away from the semipenetrable boundary, and the critical angle does not exist. When the target medium is confined in a stripe, total internal reflection occurs only when the initial angle exceeds a critical value, and the angle of reflection is a function of the stripe width, with absolute value increasing monotonically to its value for an unbounded medium [Fig. 3(d), 3(e)]. Thus the width of the target medium influences

the phenomenon of autowave total internal reflection but differently than in optics.

Reflection of autowaves has been observed by Zhabotinsky, Eager, and Epstein [12], whose results are in agreement with our theory: reflection happens only when the incident wave propagates from a less excitable to a more excitable medium, and the angle of incidence exceeds a critical value; the reflection angle is uniquely defined by the properties of the media on either side of the boundary and is independent of incident angle; and refracted and reflected autowaves never coexist. In contrast to the reflection observed in specific one-dimensional systems [30,31,46] the reflection we have described for autowaves in 2D EM is independent of the local kinetics (as far as it is generic) and is instantaneous. For those systems which exhibit reflection in 1D the refraction-reflection law will be different in a way that both reflected and refracted waves may be present at the same time and the reflected wave may appear for angles smaller than critical.

VI. CONCLUSIONS

Using kinematic theory, we have studied autowave propagation in EM with a line of discontinuity. According to our model:

(1) Autowaves which do not undergo 1D reflection also do not exhibit 2D reflection, except for total internal reflection which is independent of local kinetics.

(2) Incident and refracted autowaves obey Snell's law.

(3) The principle of reversibility in optics holds also for autowaves.

(4) Like in optics, total internal reflection occurs when the incident angle of the wave moving from the medium with slower velocity exceeds a critical angle.

(5) In contrast to optics, where the angle of incidence equals the angle of reflection, for autowaves the angle of total internal reflection is independent of incident angle (provided it exceeds the critical angle). If the target medium is confined to a stripe, the angle of reflection increases with the stripe width monotonically to the characteristic reflection angle of an unbounded target medium.

(6) In contrast to optics where refracted and reflected waves may coexist, for autowaves only one of them can exist at a time.

Our theoretical results confirm phenomena observed in experiments with chemical EM, but reliable quantitative experimental data concerning autowave refraction-reflection phenomena are not available yet.

For electromagnetic waves, the refraction index is frequency dependent (dispersion). Surface water waves change their frequency when they pass through the discontinuity line between shallow and deep water. The geometry of autowaves propagating through a semipenetrable boundary suggests that a train of planar fronts will change its frequency after being refracted at the boundary line. As a result, a boundary which is penetrable by a solitary wave may be opaque for a wave train, if the frequency of the refracted train would have to become higher than allowed by the autowave dispersion law.

The homogeneous solutions we used as building blocks are based on the eikonal approximation (7) which is not valid for curvatures close to a critical curvature $k^*_{\rm cr}>0$. Incorporating in the theory a more realistic function $V(k)$ will make impossible in some circumstances, the concatenation of a plane front with solutions (13)–(15). In other words, reflected and refracted waves will not be possible with angles close to $\pi/2$. In those cases where initial conditions would lead to such angles, the critical curvature effect will cause a break in the originally continuous front.

ACKNOWLEDGMENTS

This work was supported by NSF Grant No. CHE 95-00763.

[1] A. N. Zaikin, A. M. Zhabotinsky, Nature **225**, 535 (1970); N. A. Gorelova, J. Bares, J. Neurobiol. **14**, 353 (1983); V. L. Koroleva and J. Bures, Brain Res. **174**, 209 (1979).

[2] A. T. Winfree, *When Time Breaks Down* (Princeton University Press, Princeton NJ, 1987).

[3] A. S. Mikhailov, *Foundations of Synergetics. I. Distributed Active Systems* (Springer-Verlag, Berlin, 1990), and references therein.

[4] *Nonlinear Wave Processes in Excitable Media*, edited by A. Holden, M. Markus, and H. Othmer (Plenum, New York, 1990); *Wave and Patterns in Chemical and Biological Media*, Special Issue of Physica D **49**, No. 1&2 (1991), edited by H. L. Swinney, V. I. Krinsky.

[5] R. FitzHugh, Biophys. J. **1**, 445 (1961); J. Nagumo, S. Arimoto, and S. Yoshizawa, Proc. IRE. **50**, 2061 (1962); R. Field and R. Noyes, J. Chem. Phys. **63**, 2289 (1975).

[6] V. S. Zykov, *Simulation of Wave Processes in Excitable Media*, edited by A. T. Winfree (Manchester University Press, Manchester, 1987).

[7] W. Jahnke, C. Henze, and F. T. Winfree, Nature **336**, 662 (1988).

[8] J. P. Keener and J. J. Tyson, Physica D **21**, 307 (1986).

[9] P. Foerster, S. Muller, and B. Hess, Science **241**, 685 (1988); Development **109**, 11 (1990).

[10] R. S. Longhurst, *Geometrical and Physical Optics* (Wiley, New York, 1962); M. Born and E. Wolf, *Principles of Optics* (Pergamon, Oxford, 1970).

[11] A. C. Scott, F. Y. E. Chu, and D. W. McLaughlin, Proc. IEEE **61**, 1443 (1973).

[12] A. M. Zhabotinsky, M. D. Eager, and I. R. Epstein, Phys. Rev. Lett. **71**, 1526 (1993).

[13] O. Steinbock, V. S. Zykov, and S. C. Muller, Phys. Rev. E **48**, 3295 (1993).

[14] E. Koros, Nature, **251**, 703 (1974); J. Schutze, O. Steinbock and S. C. Muller, Phys. Rev. Lett. **68**, 248 (1992); V. Perez-Munuzuri *et al.*, Physica D **56**, 229 (1992).

[15] R. R. Aliev and A. B. Rovinsky, J. Phys. Chem. **96**(2), 732 (1992); M. Braune and H. Engel, in *Spatio-Temporal Organi-*

zation in Nonequilibrium Systems (Projekt-Verlag, Dortmund, 1992), p. 34; M. Markus, Z. Nagy-Ungavarai, and B. Hess, Science **257**, 225 (1992); A. Pertsov, M. Vinson, Philos. Trans. R. Soc. London A **347**, 687 (1994).

[16] A. M. Zhabotinsky, in *Chemical Waves and Patterns*, edited by R. Kapral and K. Showalter (Kluwer, Dordrecht, 1995), p. 401.

[17] M. Markus and K. Stavridis, Philos. Trans. R. Soc. London A **347**, 601 (1994).

[18] O. Steinbock and S. C. Muller, Physica A **188**, 61 (1992).

[19] V. A. Vavilin, A. M. Zhabotinsky, and A. N. Zaikin, Zh. Fiz. Khi. **42**, 3091 (1968) [Russ. J. Phys. Chem. **42**, 1649 (1968)].

[20] A. M. Pertsov *et al.*, Circulation Res. **72**, 631 (1993).

[21] A. M. Pertsov, E. A. Ermakova, and E. E. Shnol, Physica D **44**, 178 (1990); K. Agladze *et al.*, Science **264**, 1746 (1994); M. Gomez-Gesteira *et al.*, Phys. Rev. E **52**, 4646 (1994).

[22] K. I. Agladze, V. I. Krinsky, and A. M. Pertsov, Nature **308**, 834 (1984); J. Maselko and K. Showalter, Physica D **49**, 21 (1991); N. El-Sherif *et al.*, Circulation Res. **51**, 152 (1982).

[23] P. K. Brazhnik *et al.*, Radiophys. Quant. Electron. **31**, 419 (1988); A. M. Pertsov and Ye. A. Yermakova, Biophysics (USSR), **33**, 364 (1988); R. R. Aliev, A. B. Rovinsky, J. Phys. Chem., **96**, 732 (1992); V. N. Biktashev, A. V. Holden, Chaos, Solutions & Fractals, **5**, 575 (1995).

[24] E. A. Yermakova, A. M. Pertsov, Biophysics. (USSR) **31**(5), 855 (1986); V. N. Biktashev, in *Nonlinear Waves* 2, edited by A. V. Gaponov-Grekhov, M. I. Rabinovich, and J. Engelbrecht (Springer-Verlag, Berlin 1989), p. 87; I. Aranson, D. Kessler, and I. Mitkov, Phys. Rev. E **50**, R2395 (1994).

[25] P. K. Brazhnik, Physica D **93**, 143 (1996).

[26] P. K. Brazhnik and J. J. Tyson, Physica D (to be published).

[27] A. M. Zhabotinsky, S. C. Muller, and B. Hess, Chem. Phys. Lett. **172**, 445 (1990); A. E. Bugrim, A. M. Zhabotinsky, and I. R. Epstein, Phys. Rev. Lett. **75**(6), 1206 (1995).

[28] A. T. Winfree, *The Geometry of Biological Time* (Springer, New York, 1980); V. T. Krinsky, in *Self-Organization: Autowaves and Structures Far from Equilibrium*, edited by V. I. Krinsky (Springer, Berlin, 1984), p. 9; G. R. Ivanitskii, M. B. Medvinskii, and M. A. Tsyganov, Usp. Fiz. Nauk **164**, 801 (1994) [Sov. Phys. Usp. **37**(10), 961 (1994)]; G. Fernandez-Garcia *et al.*, Eur. J. Phys. **15**, 227 (1994).

[29] K. I. Agladze and P. de Kepper, in *Spatio-Temporal Organization in Nonequilibrium Systems*, edited by S. C. Muller and T. Plesser (Projekt Verlag, Dortmund, 1992), p. 1.

[30] V. Petrov, S. K. Scott, and K. Showalter, Philos. Trans. R. Soc. London A **347**, 631 (1994); V. Petrov, Ph.D. thesis, West Virginia State University, Morgantown, 1995.

[31] J. Kasek and M. Marek, Phys. Rev. Lett. **74**, 2134 (1995).

[32] O. A. Mornev, in *Self-Organization: Autowaves and Structures Far from Equilibrium*, edited by V. I. Krinsky (Springer-Verlag, Berlin, 1984), p. 111.

[33] Here Mornev mixes up the critical angle which stands for total internal reflection with the Brewster's angle which characterize the reflection of polarized light.

[34] V. A. Davydov, V. S. Zykov, and A. S. Mikhailov, Usp. Fiz. Nauk **161**, 45 (1991) [Sov. Phys. Usp. **34**, 665 (1991)]; Physica D **70**, 1 (1994).

[35] Since the EM recovers its properties after being excited, autowave fronts may have free ends inside the media. The evolution of free ends which often results in spiral waves is beyond the scope of this paper.

[36] P. K. Brazhnik, V. A. Davydov, and A. S. Mikhailov, Theor. Math. Phys. **74**, 300 (1988).

[37] P. K. Rashevsky, *Course of Differential Geometry* (Fizmatgiz, Moscow, 1956).

[38] P. K. Brazhnik and V. A. Davydov, Phys. Lett. A **199**, 40 (1995).

[39] V. Perez-Munuzuri *et al.*, Phys. Rev. E **51**, R845 (1995).

[40] V. Perez-Munuzuri *et al.*, Physica D **93**, 168 (1996).

[41] P. K. Brazhnik and J. J. Tyson (unpublished).

[42] A. N. Matveyev, *Principles of Electrodynamics* (Reinhold, London, 1966).

[43] P. Grindrod, M. A. Lewis, and J. D. Murray, Proc. R. Soc. London A **443**, 151 (1991).

[44] T. Yamaguchi *et al.*, J. Phys. Chem. **96**, 5831 (1991).

[45] T. Amemiya, M. Nakaiwa, T. Ohmori, and T. Yamaguchi, Physica D **84**, 103 (1995).

[46] J. Rinzel, Ann. N. Y. Acad. Sci. **591**, 51 (1990), and references therein.

[47] M. K. Ram Reddy, Zs. Nagy-Ungvarai, and S. S. Muller, J. Phys. Chem. **98**, 12 255 (1994).

[48] C. Nelson, J. Appl. Phys. **39**, 3337 (1968); M. Gotlieb *et al.*, J. Appl. Phys. **45**, 5145 (1974).

[49] C. Henze (private communication).